Available online at www.sciencedirect.com
SCIENCE DIRECT®
International Journal of Heat and Mass Transfer 48 (2005) 1462–1469
International Journal of HEAT and MASS TRANSFER
www.elsevier.com/locate/ijhmt

Distribution of heat sources in vertical open channels with natural convection

A.K. da Silva [a], G. Lorenzini [b], A. Bejan [a,*]

[a] Department of Mechanical Engineering and Materials Science, Duke University, P.O. Box 90300, Durham, NC 27708-0300, USA
[b] Department of Agricultural Economics and Engineering, Alma Mater Studiorum-University of Bologna, 50 viale Giuseppe Fanin, 40127 Bologna, Italy

Received 22 July 2004; received in revised form 23 October 2004
Available online 19 December 2004

Abstract

In this paper we use the constructal method to determine the optimal distribution and sizes of discrete heat sources in a vertical open channel cooled by natural convection. Two classes of geometries are considered: (i) heat sources with fixed size and fixed heat flux, and (ii) single heat source with variable size and fixed total heat current. In both classes, the objective is the maximization of the global thermal conductance between the discretely heated wall and the cold fluid. This objective is equivalent to minimizing temperature of the hot spot that occurs at a point on the wall. The numerical results show that for low Rayleigh numbers ($\sim 10^2$), the heat sources select as optimal location the inlet plane of the channel. For configuration (i), the optimal location changes as the Rayleigh number increases, and the last (downstream) heat source tends to migrate toward the exit plane, which results in a non-uniform distribution of heat sources on the wall. For configuration (ii) we also show that at low and moderate Rayleigh numbers ($Ra_M \sim 10^2$ and 10^3) the thermal performance is maximized when the heat source does not cover the entire wall. As the flow intensity increases, the optimal heat source size approaches the height of the wall. The importance to free the flow geometry to morph toward the configuration of minimal global resistance (maximal flow access) is also discussed.

Keywords: Constructal theory; Natural convection; Discrete heat sources; Electronics cooling

1. Introduction

Nature strikes us with countless examples of how flow systems reach equilibrium by selecting paths of least resistance for the currents that flow through them. The flows are of many kinds: fluid, heat, species, etc. [1]. The maximization of the approach to equilibrium is reflected in the shape, structure and speed of the flowing system.

The optimal shapes and structures that we see in nature are not obvious in engineering. The reason is that in engineering until recently, design was an art form. It relied on postulated (assumed) configurations based on intuition, handbooks and rules of thumb. Nature, on the other hand, constantly seeks and finds better architectures, en route to what in biology is recognized as the principle of the 'survival of the fittest'. Constructal

* Corresponding author. Tel.: +1 919 660 5309; fax: +1 919 660 8963.
E-mail address: dalford@duke.edu (A. Bejan).

0017-9310/$ - see front matter © 2004 Elsevier Ltd. All rights reserved.
doi:10.1016/j.ijheatmasstransfer.2004.10.019

Nomenclature

C	global thermal conductance, Eq. (12)
C_M	modified global thermal conductance, Eq. (13)
c_P	specific heat at constant pressure, $J\,kg^{-1}\,K^{-1}$
D	wall-to-wall spacing, m
D_0	size of heat source, m, Fig. 1
g	gravitational acceleration, $m\,s^{-2}$
H	height, m
k	thermal conductivity, $W\,m^{-1}\,K^{-1}$
L_d	length of extended inflow domain, m
L_u	length of extended outflow domain, m
L_0	size of heat source, m, Fig. 10
N	number of heat sources
P	pressure, $N\,m^{-2}$
Pr	Prandtl number
q'	heat current through one heat source, $W\,m^{-1}$
q''_0	heat flux through the heat source surface, $W\,m^{-2}$
Q'	total heat flow, $W\,m^{-1}$
$\mathbf{R}$	residual vector
Ra_M	modified Rayleigh number, Eq. (14)
Ra_*	Rayleigh number
S	spacing, m
T_{max}	maximal wall temperature, K
T_0	inlet fluid temperature, K
u	horizontal velocity component, $m\,s^{-1}$
$\mathbf{u}$	solutions vector
v	vertical velocity component, $m\,s^{-1}$
x, y	Cartesian coordinates, m

Greek symbols

α	thermal diffusivity, $m^2\,s^{-1}$
β	coefficient of volumetric thermal expansion, K^{-1}
δ_T	thermal boundary layer thickness, m
ρ	density, $kg\,m^{-3}$
ν	kinematic viscosity, $m^2\,s^{-1}$
μ	viscosity, $N\,s\,m^{-2}$

Subscripts

i	iteration index
max	maximum when $N = 1$
2m	maximum when $N = 2$
3m	maximum when $N = 3$
n	mesh index

Superscripts

$\sim$	dimensionless variables
$\wedge$	dimensionless variables

theory [1,2] has shown that there is no difference between the principle-based generation of configuration in natural and artificial flow systems, provided that the artificial structures are endowed with the freedom to morph under finiteness constraints.

The field of heat transfer augmentation has shown repeatedly how the generation of flow geometry works, and how geometry helps the flow system achieve its purpose. Fins, staggered arrangements, and ribbed channels come from the push toward greater access for heat currents in morphing geometries. In return, the new configurations use the available space to the maximum—they pack maximum heat transfer density [3–8].

The objective of the research reported in this paper is to determine the optimal distribution of discrete heat sources in an open vertical channel with natural convection. This problem has practical applications in the ventilation cooling of electronics and solar installations. These are the self-induced flows, which are caused by the chimney effect. Previous studies have shown the importance of the chimney effect in heat transfer augmentation [9–18]. In such studies, the importance of locating the heat source close to the channel entrance was recognized. However, the optimal placement of multiple heat sources in chimney flow was not considered.

Two recent studies [7,8] showed how to arrange discrete heat source mounted in a horizontal wall with forced convection, and in a vertical wall with natural convection. Both papers conducted a theoretical and numerical analysis showing that a non-uniform distribution of heat sources is the best configuration. Additionally, these studies showed that the heat source migrates toward the leading edge of the wall as the flow becomes stronger. In the present paper we consider two related problems: (i) how to arrange discrete heat sources of fixed size and heat flux, and (ii) how to arrange a single heat source of variable size and fixed total heat current in a vertical open channel in natural convection assisted by the chimney effect.

2. Mathematical formulation

Consider the two-dimensional asymmetrically discrete heated vertical channel shown in Fig. 1. The channel is cooled by a cold single-phase fluid, which is drawn into the channel at T_0. The coolant is a Newtonian fluid with constant properties. Additionally, the flow is assumed incompressible and the Oberbeck–Boussinesq approximation is used: the temperature difference between any hot spot temperature T_{max} and the cold fluid

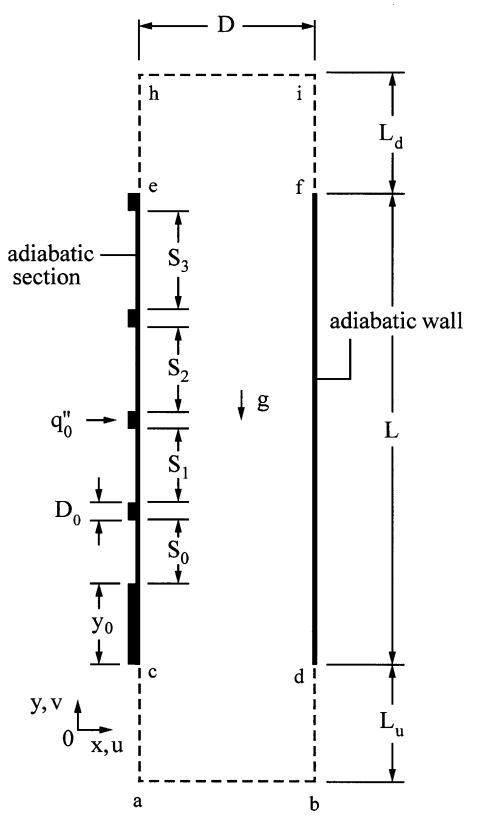

Fig. 1. Multiple length scales of the non-uniform distribution of finite-size heat sources on a vertical channel.

at T_0 is assumed small enough so that changes in density are taken into account only in the buoyancy term of the vertical momentum equation. Such considerations lead to the following differential system:

$$\frac{\partial u}{\partial x}+\frac{\partial v}{\partial y}=0 \tag{1}$$

$$\rho\left(u\frac{\partial u}{\partial x}+v\frac{\partial u}{\partial y}\right)=-\frac{\partial P}{\partial x}+\mu\nabla^2 u \tag{2}$$

$$\rho\left(u\frac{\partial v}{\partial x}+v\frac{\partial v}{\partial y}\right)=-\frac{\partial P}{\partial y}+\mu\nabla^2 v+\rho g\beta(T-T_0) \tag{3}$$

$$\rho c_P\left(u\frac{\partial T}{\partial x}+v\frac{\partial T}{\partial y}\right)=k\nabla^2 T \tag{4}$$

where $\nabla^2=\partial^2/\partial x^2+\partial^2/\partial y^2$. The variables and the fluid properties are defined in the nomenclature. Eqs. (1)–(4) were non-dimensionalized by using the variables

$$(\hat{x},\hat{y},\widehat{D},\widehat{D}_0,\widehat{S}_i)=\frac{(x,y,D,D_0,S_i)}{H} \tag{5}$$

$$(\hat{u},\hat{v})=\frac{(u,v)}{(\alpha/H)Ra_*^{1/2}Pr^{1/2}} \tag{6}$$

$$\widehat{T}=\frac{T-T_0}{q''_0H/k} \tag{7}$$

$$\widehat{P}=\frac{P}{(\mu\alpha/H^2)Ra_*^{1/2}Pr^{1/2}} \tag{8}$$

where Ra_* is the Rayleigh number based on H and the heat flux applied on each discrete heat source

$$Ra_*=\frac{g\beta q''_0H^4}{\nu\alpha k} \tag{9}$$

The numerical domain is composed of an extension upstream of the inlet ($L_u\times D$), the main channel ($D\times H$), and an extension downstream of the outlet ($D\times L_d$). The flow and temperature fields were simulated for $Pr=0.7$ in the range $10^2\leqslant Ra_*\leqslant 10^4$. The inlet and outlet extensions eliminate the need to specify inaccurate velocity or temperature profiles at the entrance and exit of the channels [19]. Instead, velocity and temperature profiles are imposed on the extremes of the domain, i.e., on the inlet and outlet planes of the extensions. The lengths of the inlet and outlet extensions (L_u, L_d) were selected such that they do not influence the variation of the hot spot temperature for the geometric configurations that were simulated. The numerical tests were performed by comparing the variation of the hot spot temperature ($\widehat{T}_{max}$) for different values of $\widehat{L}_u$ and $\widehat{L}_d$ for a fixed configuration (i.e., fixed values of $\widehat{D}$, N and $\widehat{D}_0$) through the Rayleigh number range considered in this study ($10^2<Ra_*<10^4$). By fixing $\widehat{L}_u=0$, for example, we could vary the outlet extension in the range $0\leqslant\widehat{L}_d\leqslant 1$ by using a 0.1 step in $\widehat{L}_d$. The change in $\widehat{T}_{max}$ between sequential simulations was recorded. The same procedure was adopted for $\widehat{L}_u$. The tests showed that the solution becomes relatively insensitive (i.e., the total heat transfer rate changes by less than 0.5%) when the lengths L_u and L_d are increased from $0.5H$ to H. The extensions determined in this manner and used in this study are $L_u=L_d=0.5H$. The boundary conditions are

$$\begin{aligned}
&\overline{ab}:\ \hat{u}=0 \quad\text{and}\quad \widehat{T}=0\\
&\overline{ac},\ \overline{bd} \quad\text{and}\quad \overline{fi}:\ \hat{u}=\frac{\partial\hat{v}}{\partial\hat{x}}=\frac{\partial\widehat{T}}{\partial\hat{x}}=0\\
&\overline{eh}:\ \frac{\partial\hat{u}}{\partial\hat{x}}=\frac{\partial\hat{v}}{\partial\hat{x}}=\frac{\partial\widehat{T}}{\partial\hat{x}}=0\\
&\overline{hi}:\ \frac{\partial\hat{u}}{\partial\hat{y}}=\frac{\partial\hat{v}}{\partial\hat{y}}=\frac{\partial\widehat{T}}{\partial\hat{y}}=0\\
&\overline{ce}:\ \hat{u}=\hat{v}=0,\quad \frac{\partial\widehat{T}}{\partial\hat{x}}=0 \quad\text{or}\quad \hat{q}=\frac{q}{q''_0}=1\\
&\overline{fd}:\ \hat{u}=\hat{v}=0,\quad \frac{\partial\widehat{T}}{\partial\hat{x}}=0
\end{aligned} \tag{10}$$

The numerical simulations were conducted using a commercial CFD package based on the finite element method [20]. The numerical domain was discretized non-uniformly using quadrilateral elements with 9 nodes each. The fully coupled approach, which solves all conservation equations in a simultaneous coupled manner, was used. The explicit appearance of the pressure was eliminated based on the penalty function, with an error factor of 10^{-8}. The non-linear algebraic equations resulting from the upwind finite element scheme were solved by successive substitutions followed by the Newton–Raphson scheme. The convergence criterion was controlled by two parameters: the solution vector $\mathbf{u}_i$ and the residual vector $\mathbf{R}(\mathbf{u}_i)$

$$\frac{||\mathbf{u}_i - \mathbf{u}_{i-1}||}{||\mathbf{u}_i||} \leqslant 0.001 \quad \text{and} \quad \frac{||\mathbf{R}(\mathbf{u}_i)||}{||\mathbf{R}_0||} \leqslant 0.001 \tag{11}$$

where $\|\cdot\|$ is the Euclidean norm, i is the iteration index, and $\mathbf{R}_0$ is a reference vector.

Due to the numerous simulations and the optimization objective of this work, the grid used was carefully tested and selected. The grid accuracy test was performed in the same way as for the numerical inlet and outlet extensions. The number of nodes was fixed in one direction and varied in the other until the numerical stability of $\widehat{T}_{\max}$ is reached. The grid convergence required that $\widehat{T}_{\max}$ changes by less than one percent when the grid is doubled in that direction. This procedure was used for both $\hat{x}$ and $\hat{y}$ directions. Refinement tests showed that the ideal grid is a function of the Rayleigh number, and is non-uniform in $\tilde{x}$ direction, with the smaller elements located close to the discretely heated vertical wall. The mesh accuracy study showed that the use of 101 nodes per unit of length H guarantees changes in the $T_{\max}$ solution that satisfy the grid convergence criterion throughout the range $10^2 \leqslant Ra_* \leqslant 10^4$.

3. Optimal spacings between heat sources

The optimal location of the discrete heat sources was determined by maximizing the global thermal conductance of the flow system,

$$C = \frac{Q'}{k(T_{\max} - T_0)} = \frac{N\widehat{D}_0}{\widehat{T}_{\max}} \tag{12}$$

where $Q' = Nq'$ is total heat current, k is the thermal conductivity, and $T_{\max} - T_0$ is the maximum excess temperature reached at a point (hot spot) on the left vertical wall of the channel. The position of the hot spot is free to vary, and is one of the results of the numerical optimization. When the number and size of heat sources are fixed (N, $\widehat{D}_0$), to maximize C is the same as minimizing $\widehat{T}_{\max}$.

Fig. 2 shows how the maximum temperature varies with the position of the heat source attached to vertical channel when the total heat flow is fixed. The optimal location is the one in which the heat source is located at the entrance of the channel ($\widehat{S}_{0,\text{opt}} = 0$). The same trend was found for all the other configurations in the range $10^2 \leqslant Ra_* \leqslant 10^4$ and $0.05 \leqslant \widehat{D}_0 \leqslant 0.2$. The reason for this is that the thickness of the boundary layer increases with the y-coordinate: the best place for the single heat source is the region with the thinner boundary layer, i.e., the smallest resistance.

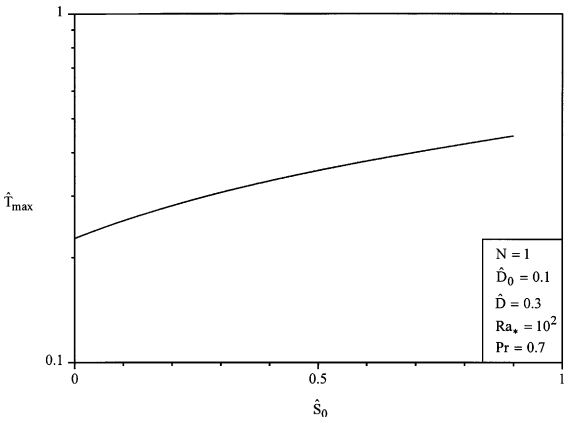

Fig. 2. Maximization of the global conductance when only one heat source is present.

Fig. 3 reports the maximized global conductance that corresponds to the optimal location of a single heat source ($N = 1$), $\widehat{S}_{0,\text{opt}} = 0$. The optimization illustrated in Fig. 2 for $\widehat{D}_0 = 0.1$ was also performed for $\widehat{D}_0 = 0.2$ and 0.05 in the Ra_* range 10^2–10^4. When $Ra_* < 10^3$, diffusive heat transfer is predominant, and $C_{\max}$ is affected weakly by $\widehat{D}_0$ and Ra_*. When $Ra_* > 10^3$, convection begins to dominate, and $C_{\max}$ increases appreciably with $\widehat{D}_0$ and Ra_*.

Next, we increased the complexity, and considered two heat sources of equal strength ($\widehat{D}_0$) installed on

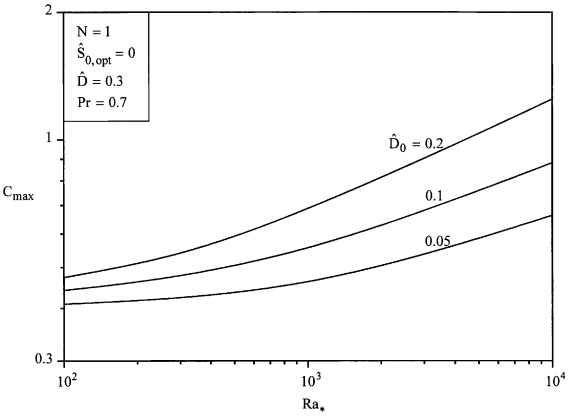

Fig. 3. The maximized global conductance that corresponds to the optimized location of one heat source.

the left wall of the channel. Consequently two degrees of freedom ($\widehat{S}_0$, $\widehat{S}_1$) have to be accounted for in order to determine the optimal configuration. The maximized conductance for this configuration is labeled C_{2m}. The optimal configuration was found by performing two nested loops: first $\widehat{S}_0$ was fixed, and C was maximized with respect to $\widehat{S}_1$, resulting in C_{max}. In the outer loop, the inner loop was repeated for several values of $\widehat{S}_0$, until C_{max} reached its highest value, C_{2m}.

As in the cases where only one heat source is active in the channel (Fig. 2), for $N = 2$ we found that $\widehat{S}_{0,opt} = 0$ throughout the range $10^2 \leqslant Ra_* \leqslant 10^4$. The new feature is that the second heat source moves along the left wall, depending on $\widehat{D}_0$ and Ra_*. As shown in Fig. 4, as Ra_* increases, the flow gains intensity and the second heat source migrates toward the exit plane of the channel. At lower values of Ra_*, the diffusion is the dominant path chosen by heat flow, consequently, the second heat source finds its own optimal location in regions with thinner boundary layer.

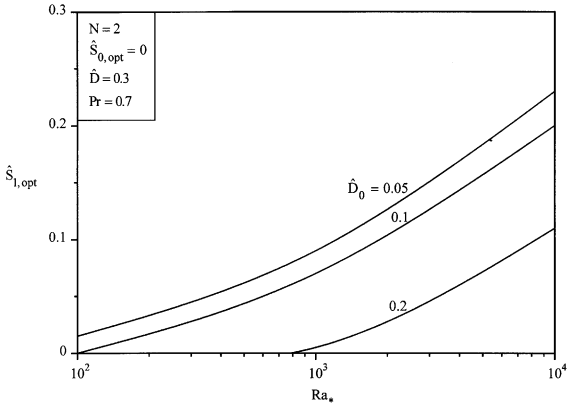

Fig. 4. The optimal location two heat sources.

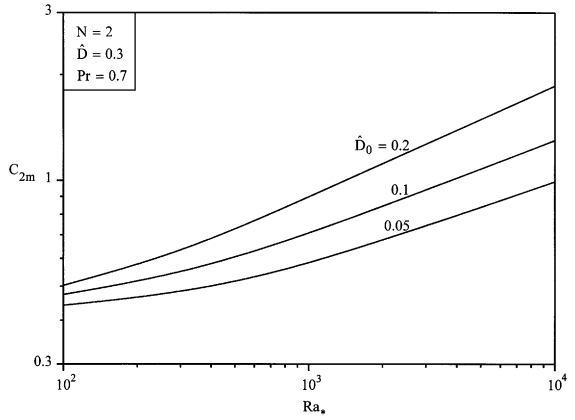

Fig. 5. The maximized global conductance that corresponds to the optimized location of two heat sources.

Fig. 5 summarizes the maximized global conductance results obtained with the two heat sources spaced optimally in Fig. 4. It is important to note that each curve shows a higher conductance than the curve for the same Ra_* and $\widehat{D}_0$ in Fig. 3. This means that increased optimized complexity yields higher performance.

Let us assume that total heat current is held constant. For $N\widehat{D}_0 = 0.1$ and $Ra_* = 10^4$, Fig. 3 shows that $C_{max} = 0.88$ when only one heat source is present $\widehat{D}_0 = 0.1$. For the same heat flow, Fig. 5 shows that $C_{2m} = 0.99$ when two optimally placed heat sources of strength $\widehat{D}_0 = 0.05$ are attached to the left wall. In conclusion, optimized complexity increases performance.

The distribution of three heat sources was optimized as shown in Fig. 6. The lower heat source always migrates toward the entrance of the channel. The new aspect is that when $N = 3$ the second heat source must also be located as close as possible to the entrance plane, for all values of $\widehat{D}_0$. This means that $\widehat{S}_{0,opt} = \widehat{S}_{1,opt} = 0$. In conclusion, the optimal spacing between heat sources with finite length exists only in configurations with two or more heat sources, $N \geqslant 2$, and occurs between the heat sources positioned closest to the exit plane. For example, when for $N = 2$ we have $\widehat{S}_{0,opt} = 0$ and $\widehat{S}_{1,opt} \neq 0$; for $N = 3$, the optimal spacings are $\widehat{S}_{0,opt} = \widehat{S}_{1,opt} = 0$ and $\widehat{S}_{2,opt} \neq 0$. Another interesting aspect is that, for a fixed value of $\widehat{D}_0$ the curves not only have the same trend, but also the same order of magnitude, $\widehat{S}_{1,N=2} \cong \widehat{S}_{2,N=3}$.

Fig. 7 shows the effect of the number of heat sources on the maximized global conductance for $N = 1$, 2 and 3 when $\widehat{D}_0 = 0.05$. The maximized global conductance increases with N. Diminishing returns are also evident: the difference between the maximized global conductance of two configurations with different N's decreases as N increases. The same behavior is shown for $\widehat{D}_0 = 0.1$ and 0.2 in Figs. 8 and 9, respectively.

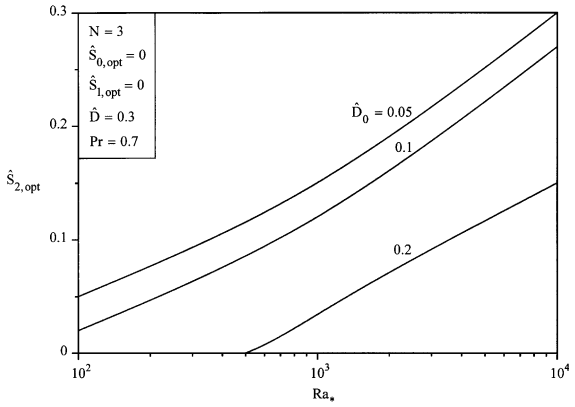

Fig. 6. Optimal location of three heat sources.

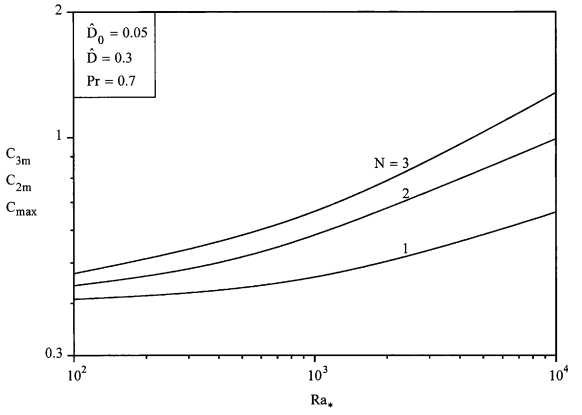

Fig. 7. The maximized global conductance that corresponds to the optimized location of three heat sources, $\widehat{D}_0 = 0.05$.

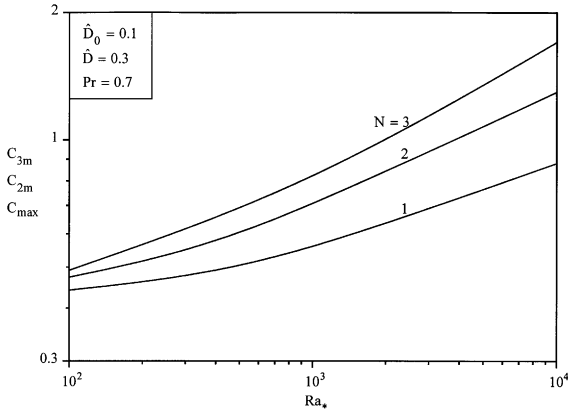

Fig. 8. Effect of N on the maximized global conductance, $\widehat{D}_0 = 0.1$.

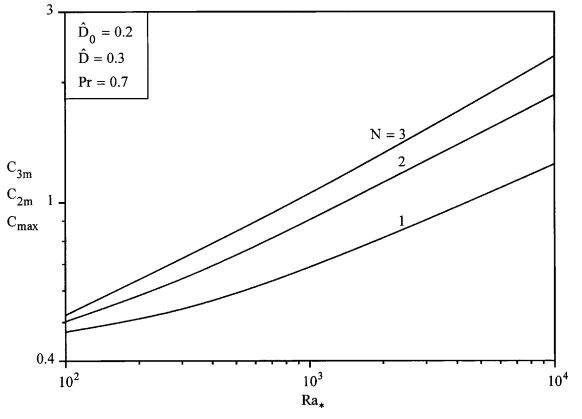

Fig. 9. Effect of N on the maximized global conductance when $\widehat{D}_0 = 0.2$.

4. Optimal intensity and position of a single heat source

In this section we consider a new configuration in order to investigate the effect of the size and position of a single heat source in natural convection. This configuration is shown in Fig. 10. Unlike in the preceding section, where each heat source had a fixed size $\widehat{D}_0$ that dissipated $\hat{q}'' = 1$, this time the only heat source present has a variable size $0 < \widehat{L}_0 < 1$ and a fixed total heat current $\hat{q}' = q'/q'_0 = 1$. This new constraint enables us to eliminate the numerator of Eq. (12) and define a modified global thermal conductance

$$C_M = \frac{q'}{k(T_{max} - T_0)} = \frac{1}{\widetilde{T}_{max}} \tag{13}$$

where $\widetilde{T}_{max}$ is the maximum dimensionless temperature based on the heat current dissipated by the heat source, $\widetilde{T} = T_{max}k/q'_0$. The remaining boundary conditions introduced in Eq. (10) continue to hold. The flow strength is indicated by a modified Rayleigh number, which is based on the heat source strength,

$$Ra_M = \frac{g\beta q'_0 H^3}{\nu\alpha k} \tag{14}$$

It is worth mentioning that the existence of an optimal heat source length may be anticipated intuitively by a skilled designer, who is able to 'see' that an

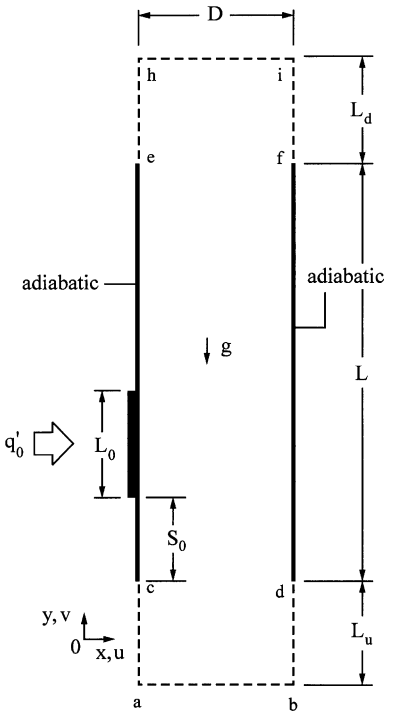

Fig. 10. Geometric parameters of a channel with single heat source of variable intensity.

optimum must exist between two extreme configurations that obey the same constraint. Intuition should not be misinterpreted as optimal design, because the latter can only be the result of an optimization process—the result of principle. Nevertheless, in principle-based optimization a premium is put on intuition (strategy) that leads more directly to optimal and nearly optimal configurations. The organization and teaching of strategy is one of the missions of constructal theory and design [1,2].

The two extremes are as follows. Because the heat current is fixed, the hot spot temperature increases greatly as $\widehat{L}_0 \to 0$. On the other hand a large heat source ($\widehat{L}_0 \to 1$) means a thick boundary layer, and consequently, a large thermal resistance. The competition between these two effects is confirmed in Fig. 11. For all the $\widehat{S}_0$ values considered, the optimal heat source length $\widehat{L}_{0,\mathrm{opt}}$ is always smaller than $(1 - \widehat{S}_0)$, meaning that when

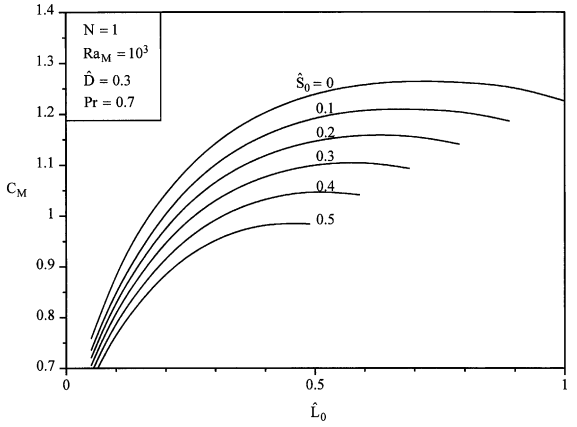

Fig. 11. Effect of the heat source size and position on the global thermal performance.

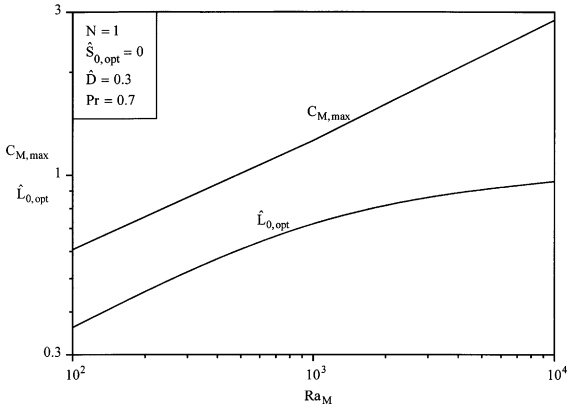

Fig. 12. Optimal heat source length and maximum global thermal performance of a channel heated by a single heat source of variable size.

$Ra_{\mathrm{M}} = 10^3$ the end of an optimized heat source never reaches the exit plane of the channel.

Fig. 12 summarizes the results for the optimal heat source length $\widehat{L}_{0,\mathrm{opt}}$ and the maximum thermal global conductance versus the modified Rayleigh number. Note that $\widehat{L}_{0,\mathrm{opt}}$ approaches 1 as the Rayleigh number increases. In the limit of high Ra_{M} the flow is strong enough to 'shave' the hot spot temperature, weakening the importance of the thickness of the boundary layer. In the limit of low Rayleigh numbers (e.g., $Ra_{\mathrm{M}} \sim 10^2$) diffusion starts to dominate the heat transfer process, and consequently $\widehat{L}_{0,\mathrm{opt}} \to 0$.

5. Conclusions

In this paper we showed numerically that the spacings between discrete heat sources of fixed size and heat flux attached to an open channel with natural convection can be optimized for maximal global thermal conductance. However, unlike in previous studies where the optimal spacing between heat sources in enclosures with natural convection and channels with forced convection decreases with the flow strength [7,8], in open channels the optimal spacing between heat sources increases with the Rayleigh number. In addition, finite-length spacings are found only in configurations with two or more heat sources, and they occur only between the heat sources positioned closest to the exit plane of the open channel. We summarized the optimal spacing between discrete heat sources in channels with forced or natural convection and in enclosures in natural convection as shown in Table 1.

The present numerical results showed that the global thermal conductance C increases with Ra^*, $\widehat{D}_0$ and N. Diminishing returns are evident as complexity increases: the stepwise gain in C decreases as N increases. Most important is that for a fixed heated coverage area $N\widehat{D}_0$, the global thermal performance increases as the number of optimally positioned heat source placed in the open channel increases.

In the second part of the paper, we showed that the position and size of a single discrete heat source with a fixed total heat current in an open channel can also be optimized for maximal global thermal performance. According to numerical results in the range $10^2 < Ra_{\mathrm{M}} < 10^4$, the optimal spacings are $\widehat{S}_{0,\mathrm{opt}} = 0$ and $\widehat{L}_{0,\mathrm{opt}} < (1 - \widehat{S}_0)$. The downstream edge of a heat source never touches the exit plane of the open channel.

In summary, the main message delivered by the present paper is that optimized complexity is a promising feature, even though diminishing returns set in as complexity increases. Optimized complexity is one of the results of the maximization of global performance in a morphing system. Optimized complexity must not be confused with maximized complexity [2].

Table 1
The optimal spacing between discrete heat sources in chimney flow

	Natural convection		Forced convection
	Open channels	Enclosures	Open channels [8]
$N = 1$	$\widetilde{S}_{0,\mathrm{opt}} = 0$	$\widetilde{S}_{0,\mathrm{opt}} \geqslant 0$	$\widetilde{S}_0 = 0$
$N = 2$	$\widetilde{S}_{0,\mathrm{opt}} = 0$ $\widetilde{S}_{1,\mathrm{opt}} \geqslant 0$ $\widetilde{S}_1$ increases with Ra_*	$\widetilde{S}_{0,\mathrm{opt}} \geqslant 0$ $\widetilde{S}_{1,\mathrm{opt}} \geqslant 0$ $\widetilde{S}_{0,\mathrm{opt}}$, $\widetilde{S}_{1,\mathrm{opt}}$ decrease with Ra_*	$\widetilde{S}_{0,\mathrm{opt}} = 0$ $\widetilde{S}_{1,\mathrm{opt}} \geqslant 0$ $\widetilde{S}_{1,\mathrm{opt}}$ decreases with Re
$N = 3$	$\widetilde{S}_{0,\mathrm{opt}} = 0$ $\widetilde{S}_{1,\mathrm{opt}} = 0$ $\widetilde{S}_{2,\mathrm{opt}} \geqslant 0$ $\widetilde{S}_{2,\mathrm{opt}}$ increases with Ra_*	$\widetilde{S}_{0,\mathrm{opt}} \geqslant 0$ $\widetilde{S}_1 \geqslant 0$ $\widetilde{S}_2 \geqslant 0$ $\widetilde{S}_{0,\mathrm{opt}}$, $\widetilde{S}_{1,\mathrm{opt}}$ decrease with Ra_*	$\widetilde{S}_0 = 0$ $\widetilde{S}_1 \geqslant 0$ $\widetilde{S}_2 \geqslant 0$ $\widetilde{S}_{1,\mathrm{opt}}$, $\widetilde{S}_{2,\mathrm{opt}}$ decrease with Re

The relationship between optimized complexity and global performance hinges on the freedom to change the configuration [21]—performance increases with the ability of the system to morph, in spite of global constraints. Freedom is to morph good design performance.

Acknowledgment

A.K. da Silva's work was fully supported by the Brazilian Research Council—CNPq under the Doctoral scholarship no. 200021/01-0.

References

[1] A. Bejan, Shape and Structure, from Engineering to Nature, Cambridge University Press, Cambridge, UK, 2000.
[2] A. Bejan, I. Dincer, S. Lorente, A.F. Miguel, A.H. Reis, Porous and Complex Flow Structures in Modern Technologies, Springer-Verlag, New York, 2004.
[3] A. Bar-Cohen, W.M. Rohsenow, Thermally optimum spacing of vertical, natural convection cooled, parallel plates, J. Heat Transfer 116 (1984) 116–123.
[4] N.K. Anand, S.H. Kim, L.S. Fletcher, The effect of plate spacing on free-convection between heated parallel plates, J. Heat Transfer 114 (1992) 515–518.
[5] T. Furukawa, W.J. Yang, Thermal optimization of channel flows with discrete heating sections, J. Non-equilibrium Thermodyn. 28 (2003) 299–310.
[6] A.K. da Silva, A. Bejan, S. Lorente, Maximal heat transfer density in vertical morphing channels with natural convection, Numer. Heat Transfer, Part A 45 (2004) 135–152.
[7] A.K. da Silva, S. Lorente, A. Bejan, Optimal distribution of discrete heat sources on a wall with natural convection, Int. J. Heat Mass Transfer 47 (2004) 203–214.
[8] A.K. da Silva, S. Lorente, A. Bejan, Optimal distribution of discrete heat sources on a wall with laminar forced convection, Int. J. Heat Mass Transfer 47 (2004) 2139–2148.
[9] W. Aung, L.S. Fletcher, V. Sernas, Developing laminar free convection between vertical plates with asymmetric heating, Int. J. Heat Mass Transfer 15 (1972) 2293–2308.
[10] J.R. Leith, Thermal design considerations in vertical-channel natural-convection, J. Heat Transfer 109 (1987) 249–251.
[11] A.G. Straarman, J.D. Tarasuk, J.M. Floryan, Heat transfer enhancement from a vertical, isothermal channel generated by chimney effect, J. Heat Transfer 115 (1993) 395–402.
[12] M. Fujii, S. Gima, T. Tomimura, X. Zhang, Natural convection to air from an array of vertical parallel plates with discrete and protruding heat sources, Int. J. Heat Fluid Flow 17 (1996) 483–490.
[13] D.A. Roberts, J.M. Floryan, Heat transfer enhancement in the entrance zone of a vertical channel, J. Heat Transfer 120 (1998) 290–291.
[14] C. Nonino, G. Lorenzini, M. Manzan, Comparisons of finite element solutions for the chimney effect between heated parallel plates, in: Progress in Engineering Heat Transfer, IFFM Publishers, 1999, pp. 415–422.
[15] F. Marcondes, C.R. Maliska, Treatment of the inlet boundary conditions in natural-convection in open-ended channels, Numer. Heat Transfer, Part B 35 (1999) 317–345.
[16] A. Auletta, O. Manca, M. Musto, S. Nardini, Thermal design of symmetrically and asymmetrically heated channel-chimney systems in natural convection, Appl. Therm. Eng. 23 (2003) 605–621.
[17] S. Kazansky, V. Dubovsky, G. Ziskind, R. Letan, Chimney-enhanced natural convection from a vertical plate: experiments and numerical simulations, Int. J. Heat Mass Transfer 46 (2003) 497–512.
[18] A. Campo, O. Manca, B. Morrone, Numerical analysis of partially heated vertical parallel plates in natural convective cooling, Numer. Heat Transfer, Part A 36 (1999) 129–151.
[19] C.R. Maliska, Computational Heat Transfer and Fluid Dynamics, Rio de Janeiro, RJ, LTC—Livros Técnicos e Científicos Ed. S.A., 1995.
[20] FIDAP Manual, Fluid Dynamics International, Inc., Evanston, IL, 1998.
[21] A. Bejan, S. Lorente, The constructal law and the thermodynamics of flow systems with configuration, Int. J. Heat Mass Transfer 47 (2004) 3203–3214.